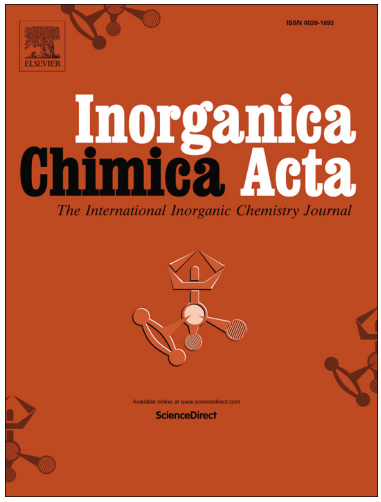

2-Hydroxyacetophenone and ethylenediamine condensed Schiff base: Fluorescent sensor for Al^{3+} and PO_4^{3-}, biological cell imaging and INHIBIT logic gate

Diganta Kumar Das, Jutika Kumar, Ananya Bhowmick, Pradip Kr. Bhattacharyya, Sofia Banu

PII: S0020-1693(16)30662-4
DOI: http://dx.doi.org/10.1016/j.ica.2017.03.003
Reference: ICA 17463

To appear in: *Inorganica Chimica Acta*

Received Date: 7 October 2016
Revised Date: 27 February 2017
Accepted Date: 2 March 2017

Please cite this article as: D.K. Das, J. Kumar, A. Bhowmick, P.K. Bhattacharyya, S. Banu, 2-Hydroxyacetophenone and ethylenediamine condensed Schiff base: Fluorescent sensor for Al^{3+} and PO_4^{3-}, biological cell imaging and INHIBIT logic gate, *Inorganica Chimica Acta* (2017), doi: http://dx.doi.org/10.1016/j.ica.2017.03.003

2-Hydroxyacetophenone and ethylenediamine condensed Schiff base: Fluorescent sensor for Al^{3+} and PO_4^{3-}, biological cell imaging and INHIBIT logic gate

Diganta Kumar Das[1]*, Jutika Kumar[1], Ananya Bhowmick[2], Pradip Kr. Bhattacharyya[3], Sofia Banu[2]

[1]Department of Chemistry, Gauhati University, Guwahati-781 014, Assam, India

[2]Department of Bio-engineering and Technology, Institute of Science and Technology, Gauhati University, Guwahati-781 014, Assam, India

[2]Department of Chemistry, Arya Vidyapeeth College, Guwahati-781 016, Assam, India

digantakdas@gmail.com

A B S T R A C T

The condensation product of 2-Hydroxyacetophenone and ethylene diamine (**L**) acts as fluorescent sensor for Al^{3+} by "off-on" mode over the metal ions –Na^{+}, K^{+}, Ca^{2+}, Mn^{2+}, Fe^{2+}, Fe^{3+}, Co^{2+}, Ni^{2+}, Cu^{2+}, Zn^{2+}, Pb^{2+}, Cd^{2+}, Hg^{2+} and Ag^{+}. The interaction of **L** with Al^{3+} results bright blue fluorescence under UV radiation and the fluorescence intensity enhances by *ca.* 40 times. The 1:1 interaction between **L** and Al^{3+}has been established from spectroscopic data as well as from DFT calculations. Snapping of photo induced electron transfer (PET) prevailed in **L,** due to interaction with Al^{3+}, is responsible for the fluorescence intensity enhancement. The detection limit and binding constant of **L** towards Al^{3+} is 10^{-5} M and $10^{5.14}$ M^{-1} respectively. **L** is applicable for determination of Al^{3+} in bovine serum albumin and for live cell imaging. The Al^{3+}:**L** complex acts as PO_4^{3-} ion sensor by fluorescent "on-off" mode over the anions – F^{-}, Br^{-}, I^{-}, NO_3^{-}, HF_2^{-}, SCN^{-}, CH_3COO^{-} and HCO_3^{2-}.**L** is found to exhibit INHIBIT logic gate behaviour with PO_4^{3-} and Al^{3+} as inputs.

Key words: Fluorescence; Aluminium; Sensor; Cell imaging, Phospahte; Logic gate

1. Introduction

8% of the total mass of the earth's crust is Aluminium (Al) which is higher than any other metal ion [1]. Modern life, in various forms (e.g. light alloys, pharmaceuticals, water purification instruments, house hold utensils etc.) depends on Al [2]. While Al in atomic form is normally not harmful, its conversion into Al^{3+}due to the environmental acidification is extremely harmful. When Al^{3+} enters human body through plants it causes Alzheimer's disease, Parkinsonism dementia, osteoporosis, colic and rickets [3]. There is report that Al^{3+}can also damage plant roots [4]. According to World Health Organization (WHO) Al^{3+} is one of the prime food pollutants and in drinking water its concentration be limited to 200 $\mu g\ L^{-1}$ (7.41 μM) [5]. WHO recommended tolerable weekly dietary human intake of Al^{3+} is 7.0 mg kg^{-1} body weight [6]. Detection of Al^{3+} in water is of environmental, biological and human health importance. At present, different detection methods, like atomic absorption and emission, spectrophotometry, electrochemiluminscence and electrochemical methods are known for detection of Al^{3+} ion [7-10]. But due to the expensive instrumentations, requirement of highly-trained operators and complicated pre-treatment makes these methods difficult for routine monitoring and applications.

Simple Schiff base ligands have gained recent interest as fluorescent sensors for metal ions including Al^{3+} due to their relatively easy one step synthesis [11–13]. Recently reported Schiff bases which act as "off-on" fluorescent sensor for Al^{3+} are based on – thiazole and salicylaldehyde [14]; 2-hydroxyethylether-2-nitrophenol and salicylaldehyde [15], 8-hydroxyjulolidine-9-carboxaldehyde and benzohydrazide [16]; 2-hydroxyaniline and 2 hydroxybenzaldehyde [17]; salicylhydrazide and ortho-phthalaldehyde [18]; salicylaldehyde and 4,4-difluoro-4-bora-3a,4a-diaza-s-indacene [19]; thiophene-2-carboxylic acid hydrazide [20]; 8-hydroxyquinoline-7-carbal- dehyde and 4-aminopyrine [21]; 2-methyl quinoline-4-carboxylic hydrazide and 8-formyl-7-hydroxyl-4-methyl coumarin [22]; perylenebisimide and di(2-(salicylideneamino))ethylamine [23]; 4-aminoantipyrine and salicylaldehyde, 4-aminoantipyrine and 2-hydroxy-1-naphthaldehydeantipyridine [24]; Rhodamine ethylenediamine and 1,8-naphthalic anhydride [25] etc.

Excess phosphate ion (PO_4^{3-}) in water leads to increased algal growth, eutrophication, and reduced water quality [26]. The excess of phosphate in human body results in kidney failure, while its deficiency leads to hyperthyroidism [27]. Fluorescent sensors are known for PO_4^{3-} which adopted different approaches - PO_4^{3-} was reacted with molybdate under acidic conditions to produce molybdophosphate which forms non-fluorescent complex with Rhodamine 6G [28]; Azodiimine based "off-on" sensor

involving ESPT [29]; Pyrene appended benzimidazolium-based simple cleft [30]; competition of PO_4^{3-} with tannic acid-stabilized Cu nanoclusters for Eu^{3+} binding [31]; carbon dots [32]; 9-Anthraldehyde nanoparticles in aqueous suspension [33]; combined effect of metal-organic frameworks and ZnO quantum dot [34]; organic ligands coated Ag nanoparticles to quench fluorescence by Cu^{2+}/Fe^{3+} and regain it by PO_4^{3-} [35]; supramolecular interaction of 1,3,5-triethylbenzene core with PO_4^{3-} [36] etc. Dual fluorescent sensor for Al^{3+} and PO_4^{3-} is rare and only rhodamine B based sensor was developed to detect Al^{3+} by "off-on" mode and the resulting complex could detect PO_4^{3-} by "on-off" mode [37]. Schiff base type isophthaloyl salicylaldehyde hydrazine moiety selectively detected Al^{3+} and PPi with "off-on" mode at two different wavelengths in aqueous solution and exhibited INHIBIT and EXOR gates [38]. Other Al^{3+} based fluorescent molecular switches are also recently reported [39, 40].

In present day, density functional theory (DFT) has become an effective tool for determining molecular structures, interaction energy and other electronic properties of molecules [41-46]. Herein we have employed DFT method to ascertain the binding pattern in the Al^{3+}:**L** complex. The geometry has been optimized using 6-31+G(d) basis set, with Becke three-parameter exchange and Lee, Yang and Parr correlation functional, B3LYP [47] and has been confirmed by the absence of imaginary frequency.

In this paper, we report that the sensor obtained from the condensation product of 2-Hydroxyacetophenone and ethylene diamine detects Al^{3+} by fluorescence "on" mode and shows bright blue fluorescence under UV radiation. The binding stoichiometry, binding constant and detection limit of the sensor towards Al^{3+}has been established from spectroscopic data and DFT calculations. The sensor is applicable for Al^{3+} in BSA as well as in live cell imaging. PO_4^{2-} detection in presence of other anions by the sensor: Al^{3+} complex is also reported.

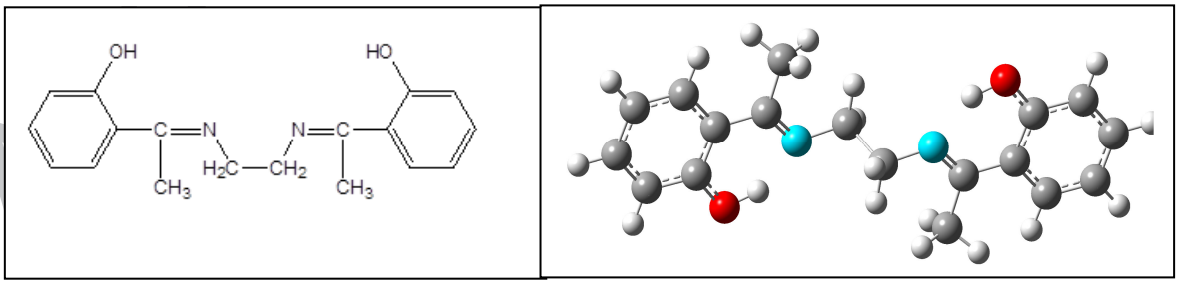

Scheme 1: Chemical structure of **L** and DFT optimised structure of **L** in more stable trans form

2. Experimental

2.1 Chemicals and experimental techniques

All the chemicals were purchased from Merck and except $Pb(NO_3)_2$, $AgNO_3$, $CaCl_2$ the other metal salts are sulphates. The metal salts were recrystallized from double distilled water before use. Solutions of **L**(5.0×10^{-4} M) and metal salts (10^{-2} M) were prepared in 1:1 (v/v) CH_3OH:H_2O.

UV/Visible spectra were recorded in a Shimadzu UV 1800 spectrophotometer using 1 cm path length quartz cuvette. ^{1}H NMR spectra were recorded in a BrukerUltrashield 300 MHz spectrometer using $CDCl_3$ as solvent and the chemical shifts were reported in δ values (ppm) relative to tetramethylsilane (TMS). Fluorescence spectra were recorded in Hitachi 2500 spectrophotometer using quartz cuvette of 1 cm path length. The FT-IR spectra were recorded in a Perkin Elmer RXI spectrometer. High resolution mass (HRMS) spectra were recorded on an Agilent spectrometer using HPLC methanol as the solvent.

2.2 Synthesis and characterisations of the sensor, L

L (2-[2-(E)-(2-hydroxyphenyl)ethylidene]aminoethyl)-ethanimidoyl] phen) was synthesized based on the reported procedure [48]. A solution of 2- hydroxyacetophenone (6 mL, 0.05 m mol) was prepared in 50 mL absolute ethanol. Ethylenediamine (3.38 mL, 0.05 m mol) was added to this solution drop wise. The reaction mixture was refluxed for 3 hours. Yellow coloured precipitate was obtained which was filtered, recrystallized from ethanol and then dried under vacuum (melting point 199.8^{o}C, yield 90%).
ESI-MS:$[M]^+$ m/z, 296.49 ($C_{18}N_2H_{20}O_2$, 100% abundance); **FT-IR** (KBr): 1610.56 cm^{-1} ($\nu_{C=N}$), 3446 cm^{-1} (ν_{O-H}), 1292.31 cm^{-1} (ν_{O-H}, bending), 2931.80cm^{-1} (ν_{C-H}, aliphatic) and 1508.33 ($\nu_{C=C}$, aromatic). **^{1}HNMR** ($CDCl_3$, δ ppm, TMS): 2.396 (s, 6H), 3.994 (s, 4H), 6.774-7.545 (m, 8H). **^{13}C NMR**: ($CDCl_3$, δ ppm, TMS): 173.53, 163.39, 132.66,129.13, 119.42, 118.21, 117.31, 49.80, 15.06

2.3 Biological cell imaging studies

Rat L6 myoblasts were grown in DMEM medium supplemented with 10% Fetal Bovine Serum (FBS), 1 % penicillin–streptomycin and maintained at 37 °C in a humidified atmosphere with 5% CO_2. For in vitro imaging study the cells were seeded in a 6 well (35 mm) culture dish with a seeding density of 3×10^5 cells per dish. After reaching 60% confluence, cells were washed with PBS and incubated in serum free media which was supplemented with $Al_2(SO_4)_3$ (100 μM) for 40 hours. Cells were then

observed under a fluorescence microscope using a 20× objective with excitation and emission filters of 370 nm and 465 nm respectively. The images were taken through an attached CCD camera. Al^{3+} treated cells were then washed with PBS and further incubated with **L (50** μM) for 3 hours and observed under fluorescence microscope.

3. Results and discussion

*3.1 Fluorescence detection of Al^{3+} by **L***

Insert Figure 1 Here

L (5×10^{-4} M) in 1:1 (v/v) CH_3OH:H_2O showed weak fluorescence emission in the range 380 nm to 700 nm when excited with 370 nm photons. The addition of Al^{3+} to the solution of **L** was found to increase the fluorescence intensity with associated red shift (Fig. 1, Scheme 2). The final fluorescence peak was observed at λ_{max}=464 nm when Al^{3+}:**L** concentration ratio became 1:1. Fig. 1B shows the plot of I/I_o versus Al^{3+} concentration where I is fluorescence intensity at a particular concentration of Al^{3+} and I_o is the fluorescence intensity of **L** at zero Al^{3+} concentration. The I/I_o value gradually increased and became *ca.* 40 when the concentration ratio of Al^{3+} and **L** reached 1:1, further addition of Al^{3+} did not change the I/I_o value.

Scheme 2: **L** (left) and **L**+Al^{3+}(right) in 1:1 (*v/v*) 1:1 (v/v) CH_3OH:H_2O under UV light of 365 nm

Similar fluorescent spectral titrations were performed with metal ions – Na^+, K^+, Ca^{2+}, Cr^{3+}, Mn^{2+}, Fe^{2+}, Fe^{3+}, Cu^{2+}, Co^{2+}, Ni^{2+}, Zn^{2+}, Cd^{2+}, Hg^{2+}, Pb^{2+}, Mg^{2+} and Ag^+ but no appreciable change in fluorescence characteristics of **L** was observed. The effect of different metal ions on the relative fluorescence intensity (I/I_o) of **L** has been shown in Fig. 2 through bar diagram. From the diagram it is clear that **L** can clearly distinguish Al^{3+} over the other metal ions. Here I_o and I are the fluorescence intensities of **L** at zero and at one equivalent concentration of other metal ion respectively in the solution.

Insert Figure 2 Here

Insert Figure 3 Here

The selectivity of **L** towards Al^{3+} in the presence of other metal ions has been done. For this purpose fluorescence intensity of **L** in presence of one equivalent of a metal ion Na^+, K^+, Ca^{2+}, Cr^{3+}, Mn^{2+}, Fe^{2+}, Fe^{3+}, Cu^{2+}, Co^{2+}, Ni^{2+}, Zn^{2+}, Cd^{2+}, Hg^{2+}, Pb^{2+}, Mg^{2+} and Ag^+ was recorded. Then one equivalent of Al^{3+} was added to the solution already containing one equivalent metal ion and the fluorescence intensity was observed after 5 minutes of standing. The fluorescence intensity was enhanced with the almost same I/I_0 ratio that was observed when only Al^{3+} ion was present (Fig. 3).

The interaction between **L** and Al^{3+} was also confirmed by UV-Visible spectroscopy. The UV-Visible spectra of 5×10^{-4} M **L**in 1:1 (v/v) $CH_3OH:H_2O$ has been recorded at different added concentration of Al^{3+} (Fig. 4). Absorption maxima for **L** in 1:1 (v/v) $CH_3OH:H_2O$ were observed at λ_{max} 386 nm, 327 nm and 276 nm (sh). With the addition of Al^{3+} the absorbance peak at 386 nm and 327 nm gradually shifted by 10 nm towards lower wavelength that is blue shift occurred with a decrease in absorbance.

Insert Figure 4 Here

The fluorescence data have been used to determine the binding stoichiometry and binding constant between L and Al^{3+} through the plot of $\log[(I_o–I)/(I–I_{final})]$ versus $\log[Al^{3+}]$[28,29] (Fig. 5). I_o, I and I_{final} are the fluorescence intensities of **L** in absence of Al^{3+},at an intermediate concentration of Al^{3+} and at one equivalent concentration of Al^{3+} respectively. The slope of the plot was found to be 1.18 indicating that oneAl^{3+} binds to one **L** and the binding constant (β) was found as $\log\beta = 5.14$.The detection limit was determined from the $(I-I_0)$ versus $\log[Al^{3+}]$ plot and was found to be 10^{-5} M.[74]

Insert Figure 5 Here

The Al^{3+} induced fluorescence "off–on" behavior of **L** could be explained on the basis of the photoinduced electron transfer (PET) mechanism. In **L** the PET occurs from the lone pair electron density on immine N atoms to the phenyl rings. Binding of Al^{3+} to the N atoms of **L** snaps this PET process leading to fluorescence enhancement.

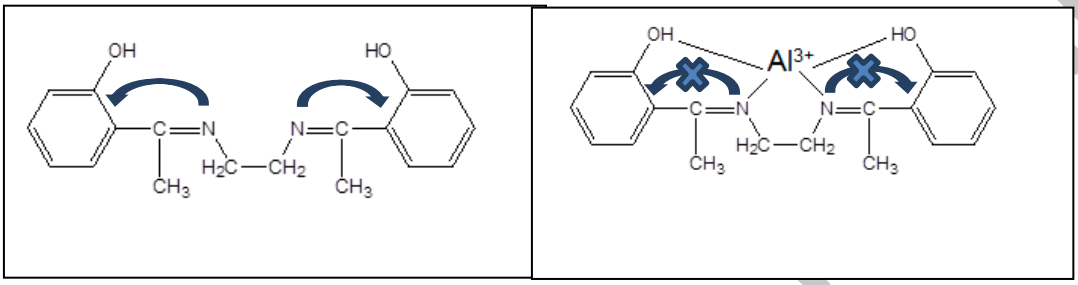

scheme 2: (A) PET from N lone pair to the benzene rings and (B) Snapping of PET due to binding of **L** with Al^{3+} through N lone pairs electrons

In order to substantiate the PET mechanism and hence the involvement of N lone pair electron density for bond formation with Al^{3+} we recorded, in solution, the FT-IR and HRMS of the Al^{3+}:**L** complex. Before recording the FT-IR spectrum or HRMS the completeness of complex formation was checked by recording the fluorescence spectra, which showed *ca.* 40 times increase in fluorescence intensity. The observed significant change in the FT-IR spectrum recorded was that the 1610 cm^{-1} peak of **L** due to $\nu_{C=N}$ shifted to 1653 cm^{-1}. The HRMS spectrum of the Al^{3+}:**L** complex showed molecular ion peak at 324 which confirms the formation of the complex.

3.2 Reversibility of L towards Al^{3+}

Insert Figure 6 Here

The fluorescence intensity enhancement of **L** on interaction with Al^{3+} was found to be reversible. When the strong metal ion chelator disodium salt of ethylenediaminetetraacetate (Na_2EDTA) was added gradually to a 1:1 mixture of Al^{3+}:**L** the already enhanced fluorescence intensity of the solution was found to decrease till it reaches the original fluorescence intensity of **L**. Fig. 6 shows the effect of $EDTA^{2-}$ on the fluorescence spectra of Al^{3+}**L**. The Al^{3+} of the complex was removed by $EDTA^{2-}$ through chelation leaving free **L** and hence fluorescence intensity was lowered.

3.3 DFT Calculations

The structure of **L** as well as **L:**$Al^{3+}$was optimised using 6-31+G(d) basis set, with Becke three-parameter exchange and Lee, Yang and Parr correlation functional, B3LYP[75]and was confirmed by the absence of imaginary frequency. In case of **L** two orientations were possible, one trans and the other cis with the former being more stable (Fig. 7). However, in the **L:**Al^{3+} complex the two N of **L** are at the cis positions which is (in gas phase) 0.94 kcal/mol more stable compared to the corresponding trans complex (Fig. 8). The calculated values of different bond lengths and bond angles are included in Table 1 which supports that the complex acquired a distorted planar structure.

Insert Figure 7 Here

Insert Figure 8 Here

As the complex formation is taking place in solvent phase (1:1 methane-water) we further observed the effect of the solvent phase on the structure of the complexes. For this purpose we optimized the gas phase structure in solvent phase (in methanol and water) using the same level of theory. It is interesting to note that the solvent phases do not impart any significant impact on the structures (the bond lengths are varied by ~0.02 Å and bond angles by 1º-2º only), **Supplement table 1**.

3.4 Determination of Al^{3+} in bovine serum albumin

Insert Figure 9 Here

The sensor **L** was successfully utilized for the determination of Al^{3+} in aqueous solution of bovine serum albumin (BSA). Fig. 9A shows the fluorescence intensity enhancement for **L** in BSA medium upon interaction with Al^{3+}. Fig. 9B, inset shows the plot of I/I_o as a function of Al^{3+} concentration. An enhancement in fluorescence intensity of *ca.* 34 times has been observed at 1:1 concentration ratio of **L** and Al^{3+}. This value is comparable to the I/I_o value of 40 in case of water. The same experiment was repeated with biologically relevant fluorescence excitation at 410 nm. A gradual increase in fluorescence intensity with increasing Al^{3+} concentration was observed (Fig. 9B) at this excitation too. Thus **L** is applicable for determination of Al^{3+} in aqueous solution of BSA.

3.5 Living biological cell imaging studies

Insert Figure 10 Here

Figure 10 shows the fluorescence sensing ability of **L** to detect Al^{3+} in live Rat L6 myoblasts cells. Panel [A] shows the fluorescent microscopic image of live Rat L6 myoblasts cells in PBS, panel [B] shows the fluorescent microscopic image of live Rat L6 myoblasts cells incubated with **L** in PBS, panel [C] shows the fluorescent microscopic image of live Rat L6 myoblasts cells incubated with Al^{3+} in PBS. No fluorescent spot was observed in these panels. When both **L** and Al^{3+}were incubated with live Rat L6 myoblasts cellsin PBS bright circular spots were observed as shown in panel [D] of Fig. 10. This clearly proves that our developed sensor **L** is applicable for Al^{3+} detection in live biological cells.

Reversibility of Al^{3+} and **L** interaction with respect to Na_2EDTA was also performed in cells. The bright spots shown in panel D was found to gradually fade with the addition of Na_2EDTA and finally disappear at 1:1 concentration ratio of Al^{3+} and Na_2EDTA (Panel E, Fig. 10).

3.6 Fluorescent "on-off" sensing of PO_4^{3-} by Al^{3+}L complex

Insert Figure 11 Here

The fluorescent Al^{3+}L complex in 1:1 *v/v* CH_3OH:H_2O was tested for anion sensing and found to show positive result towards PO_4^{3-} ion by fluorescent "on-off" mode. Fig. 11 shows that with increasing PO_4^{3-}anion concentration the fluorescence intensity of L:Al^{3+} complex deceases and becomes minimum when PO_4^{3-}anion concentration becomes three equivalents. Similar fluorescence titration with anions – HPO_4^{2-}, $H_2PO_4^-$, HCO_3^{2-}, NO_3^-, F^-, Cl^-, Br^-, I^-, SCN^-, H_2F^- and CH_3COO^- resulted insignificant change in fluorescence intensity of the Al^{3+}L complex in 1:1 *v/v*CH_3OH:H_2O. Fig. 12 depicts the I/Io values of Al^{3+}L complex through bars in 1:1 *v/v* CH_3OH:H_2O on interaction with these anions together with PO_4^{3-} anion. From this figure it is clear that the Al^{3+}L complex can distinguish PO_4^{3-} anion over HCO_3^{2-}, NO_3^-, F^-, Cl^-, Br^-, I^-, SCN^-, H_2F^- and CH_3COO^- by fluorescence "off-on" mode.

Insert Figure 12 Here

Insert Figure 13 Here

Selectivity of $Al^{3+}L$ complex towards PO_4^{3-} anion in presence of another anion was also judged by recording fluorescence spectra of $Al^{3+}L$ complex in presence of PO_4^{3-} anion and another anion. Fig. 13 compares through bars the I/Io values of $Al^{3+}L$ + PO_4^{3-} anion and $Al^{3+}L$ + PO_4^{3-} anion + another anion. The comparable height of the bars in both the cases confirms that $Al^{3+}L$ complex is selective towards PO_4^{3-} anion even in presence of another anion.

3.7 INHIBIT logic gate behaviour of L

Insert Figure 14 Here

Based on the two different fluorescence emission states "on" or "off", the sensor **L** has been analysed with a molecular logic gate considering the two inputs PO_4^{3-} and Al^{3+} as input "a" and input "b" respectively. Input value "1" means presence and input "0" means absence of the input. Similarly out put "1" means presence and "0" means absence of fluorescence when **L** interacts with the input. The logic truth table has been illustrated in Fig. 14. Only the addition of Al^{3+}led to fluorescence emission of **L** which is not observed when both Al^{3+} and PO_4^{3-} are present leading to an INHIBIT (INH) logic gate.

4. Conclusion

In summary, we have reported a new fluorescent sensor for Al^{3+} by fluorescent "on" mode which is highly selective over the metal ions - Na^+, K^+, Ca^{2+}, Mn^{2+}, Fe^{2+}, Fe^{3+}, Co^{2+}, Ni^{2+}, Cu^{2+}, Zn^{2+}, Pb^{2+}, Cd^{2+}, Hg^{2+} and Ag^+. The detection limit and binding constant of the sensor towards Al^{3+} is 10^{-5} M and $10^{5.14}$ M^{-1} respectively. The sensor:Al^{3+} complex acts as sensor for PO_4^{3-} ion by fluorescent "off" mode and is selective over anions - F^-, Br^-, I^-, NO_3^-, HF_2^-, SCN^-, CH_3COO^- and HCO_3^{2-}. The sensor has been applied for fluorescent detection of Al^{3+} in live Rat L6 myoblasts cells and in bovine serum albumin. The sensor has been found to act as INHIBIT logic gates for Al^{3+} and PO_4^{3-} ion as input.

Acknowledgement

The authors thank UGC, New Delhi and DST, New Delhi for financial assistance to the department under DSA and FIST-II programme, respectively. INFLIBNET (UGC) is thanked for literature survey help and IIT-Guwahati is thanked for HRMS data.

References

[1] S. Goswami, S. Paul, A. Manna, RSC Adv. 3 (2013) 10639.

[2] S. V. Verstraeten, L. Aimo, P. I. Oteiza, Arch. Toxicol. 82 (2008) 789.

[3] B. Wang, W. Xing, Y. Zhao, X. Deng, Environ. Toxicol.Pharmacol. 29 (2010) 308.

[4] E. Delhaize, P. R. Ryan, Plant.Physiol. 107 (1995) 315.

[5] T. Han, X. Feng, B. Tong, J. Barcelo, C. Poschenrieder, Environ. Exp. Bot., 48 (2002) 75.

[6] L. Shi, L. Chen, J. Zhi, T. Dong, Chem. Commun. 48 (2012) 416.

[7] H. Sang, P. Liang, D. Du, J. Hazardous Materials 154 (2008) 1127.

[8] S. J. Djane, M. Gra, C. Korn, Spectrochim.Acta Part B, 55 (2000) 389.

[9] S. Abbasi, A. Farmany, Food Chemistry 116 (2009) 1019.

[10] V. K. Gupta, A.K. Jain, G. Maheshwari, Talanta, 72 (2007) 1469.

[11] K. Dutta, R.C. Deka, D.K. Das, J. Lumin., 148 (2014) 325.

[12] D.K. Das, P. Gos.wami, B. Medhi, J. Fluoresc., 145 (2014) 454.

[13] J. Kumar, P. Bhattacharyya, D.K. Das, Spectrochim.Acta A, 138 (2015) 99.

[14] V. K. Gupta, A. K. Singh and L. K. Kumawat, Sens. Actuators B, 195 (2014) 98.

[15] C.H. Chen, D.J. Liao, C.F. Wan, A.T. Wu, Analyst, 138 (2013) 2527.

[16] S.A. Lee, G.R. You, Y.W. Choi, H.Y. Jo, A.R. Kim, I. Noh, S.J. Kim, Y. Kim, C. Kim, Dalton Trans., 43 (2014) 6650.

[17] S. Kim, J.Y. Noh, K.Y. Kim, J.H. Kim, H.K. Kang, S.W. Nam, S.H. Kim, S. Park, C. Kim, J. Kim, Inorg. Chem., 51 (2012) 3597.

[18] L. Wang, W. Qin, X. Tang, W. Dou, W. Liu, Q. Teng, X. Yao, Org. Biomol. Chem., 8 (2010) 3751.

[19] R. Kang, X. Shao, F. Peng, Y. Zhang, G. T. Sun, W. Zhaoa, X.D. Jiang, RSC Adv., 3 (2013) 21033.

[20] K. Tiwari, M. Mishra, V. P. Singh, RSC Adv., 3 (2013) 12124.

[21] L. Fan, X. Jiang, B. Wang, Z. Yang, Sens. Actuators B, 205 (2014) 249.

[22] J. Qin, T. Li, B. Wang, Z. Yang, L. Fan, Spectrochim.Acta A, 133 (2014) 38.

[23] S. Malkondu, Tetrahedron, 70 (2014) 5580.

[24] V. K. Gupta, A.K. Singh, N. Mergu, Electrochim.Acta, 117 (2014) 405.

[25] S Paul, A Manna, S Goswami, Dalton Trans. 44 (2015) 11805.

[26] H. Cao, Z. Chen and Y. Huang, Talanta, 2015, 143, 450.

[27] B.P. Morgan, S. He, R.C. Smith, Inorg. Chem., 46 (2007) 9262.

[28] L. Kroeckel, H. Lehmann, T. Wieduwilt, M. A. Schmidt, Talanta, 125 (2014) 107.

[29] C. Kar, S.K. Dey, G. Das, *Sensor Letters*, 9 (2011) 1430.

[30] K. Ghosh, D. Kar, P. R. Chowdhury, Tetrahedron Letters, 52 (2011) 5098.

[31] H. Cao, Z. Chen, Y. Huang, Talanta 143 (2015) 450.

[32] J. Xu, Y. Zhou, G. Cheng, M. Dong, S. Liu, C. Huang, J. Luminesce., 30 (2015) 411.

[33] P. G. Mahajan, N.K. Desai, K. Netaji, D. K. Dalavi, D. P. Bhopate, G. B. Kolekar, B. Govind, S. R.Patil, *J. Fluoresce.* 25 (2015) 31.

[34] D. Zhao, X. Wan, H. Song, L. Hao, S. Liying, Lv Y. Yingying, Sensors and Actuators B, 197 (2014) 50.

[35] N. Kaur, S. Kaur, A. Kaur, P. Saluja, H. Sharma, A. Saini, N. Dhariwal, A. Singh, N. Singh, J. Luminesce. 145 (2014) 175.

[36] N. A. Esipenko, P. Koutnik, T. Minami, L. Mosca, V. M. Lynch, G. V. Zyryanov, P. Anzenbacher, Chem. Sc., 4 (2013) 3617.

[37] X. Wan, L. Xuejuan, T. Liu, H. Liu, L. Gu and Y. Yao, RSC Adv., 2014, 4, 29479.

[38] S Goswami, A Manna, S Paul, K Aich, A K Das, S Chakraborty, Dalton Trans. 42 (2013) 8078.

[39] S Goswami, A Manna, S Paul, A K Maity, P Saha, C K Quah, H-Kun Fun RSC Adv. 4 (2014) 34572.

[40] S Goswami, S Paul and A Manna RSC Adv. 3 (2013) 25079

[41] C. Cramer J. Essentials of Computational Chemistry, Theories and Models, 2nd Ed., John Wiley & Sons Ltd, England, 2004.

[42] W. M. Koch, C. Holthausen, A. Chemist's Guide to Density Functional Theory, 2nd Ed. Wiley-VCH, New York, 2001.

[43] C. Fiolhais, F. Nogueira, M. (Eds.) Marques , A Primer in Density Functional Theory, Springer-Verlag, Berlin, 2003.

[44] J. Aron, P. M-S Cohen, Y. Weitao, Chem. Rev., 112 (2012) 289.

[45] C.P. Robert, Annu. Rev. Phys. Chem. 46 (1995) 701.

[46] J. Kumar, M.J. Sarma, P. Phukan, D.K. Das, J. Fluoresce. 25 (2015) 1431.

[47] A.D. Becke, J. Chem. Phys., 98 (1993) 5648.

[48] A.M . Hamil, M. Abdelkarem, M. Hemmet, M. El-ajaily M, International J. Chem. Tech. Res., 4 (2012) 682.

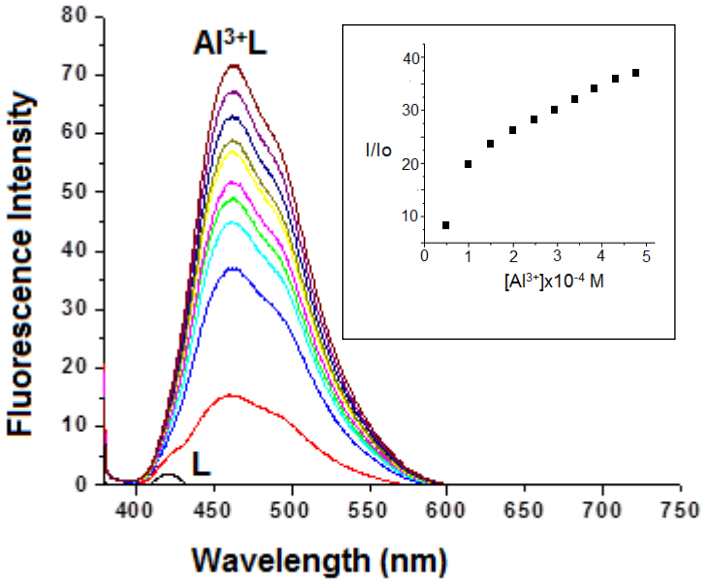

Fig. 1- Fluorescence emission spectra of **L** (50 μM) in 1:1 (v/v) CH_3OH-H_2O upon addition of 0, 5, 10, 15, 20, 25, 30, 35, 45 and 50 μM Al^{3+} (λ_{em} 464 nm, λ_{ex} 370 nm). Inset: Plot of I/Io versus Al^{3+} concentration.

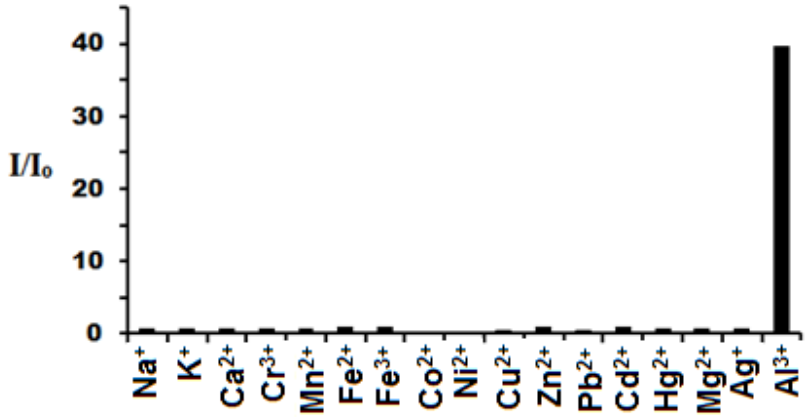

Fig. 2 Bar diagram showing the effect of different metal ions on I/I_o values of **L**in1:1 (*v/v*) CH_3OH-H_2O.

.

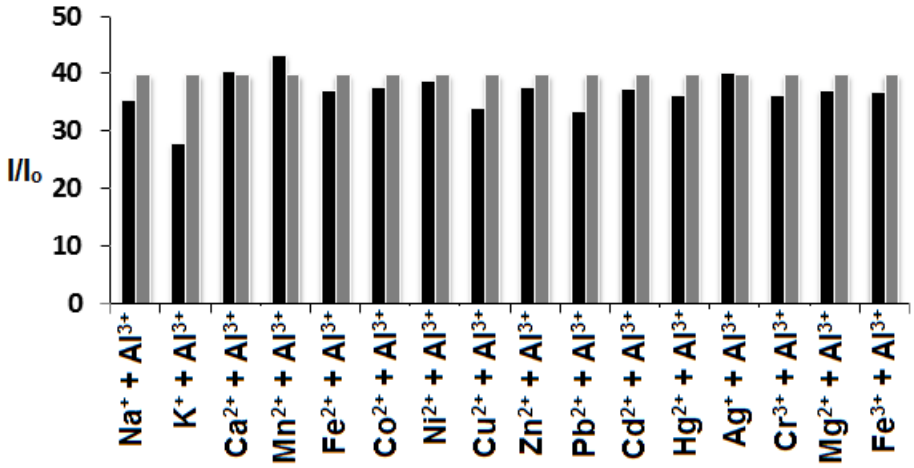

Fig. 3 I/I_o response of **L** in the presence of (i) Al^{3+}(grey bars); (ii) Al^{3+} in presence of another metal ion (black bars) in 1:1 (*v/v*) CH_3OH-H_2O. Similar heights of black and grey bars confirm selectivity of **L** towards Al^{3+}over another metal ion.

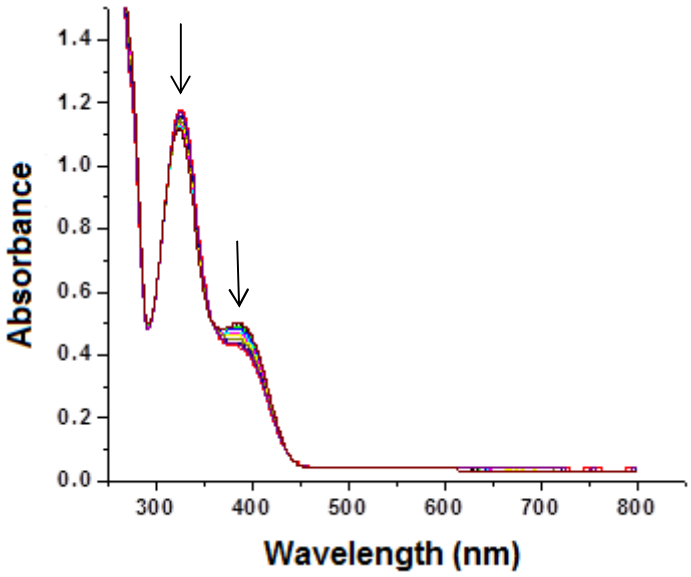

Fig. 4- Change in the UV/Visible spectra of **L** (50 μM) as a function of added Al^{3+} (5-50 μM) in 1:1 (*v/v*) CH_3OH-H_2O.

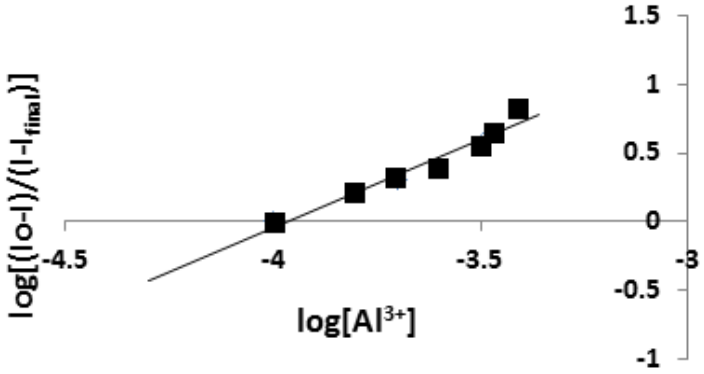

Fig. 5- Plot of $\log[(I_o–I)/(I–I_{final})]$ versus $\log[Al^{3+}]$ for **L** and Al^{3+} interaction in 1:1 (*v/v*) CH_3OH-H_2O.

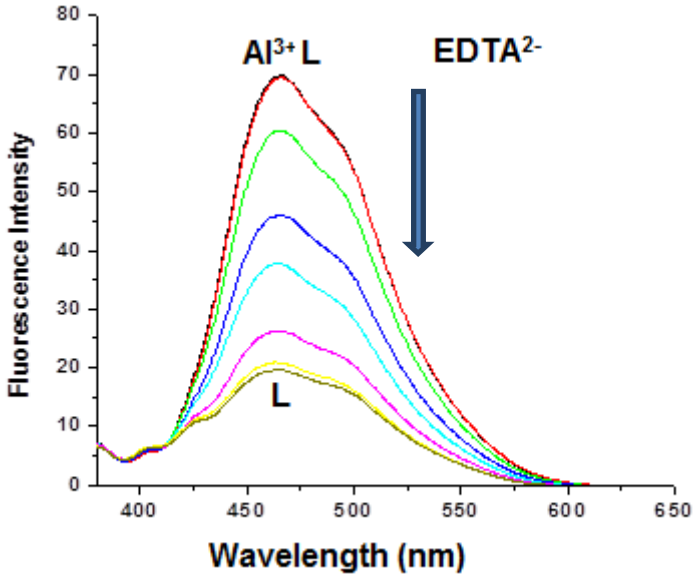

Fig. 6: Decrease in fluorescence intensity of $Al^{3+}L$ complex with the addition of $EDTA^{2-}$ in 1:1 (*v/v*) CH_3OH-H_2O.

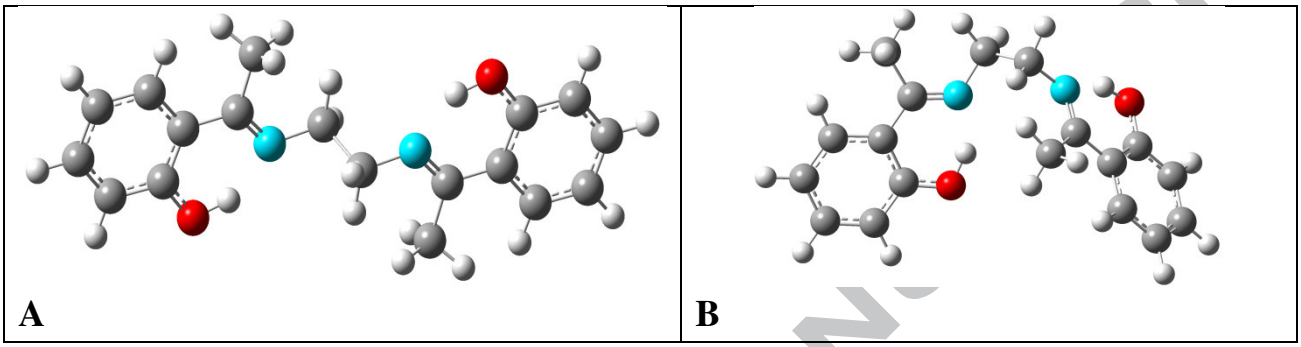

Fig. 7: DFT optimised structure of **L** when- N atoms are trans [A] and N atoms are cis [B].

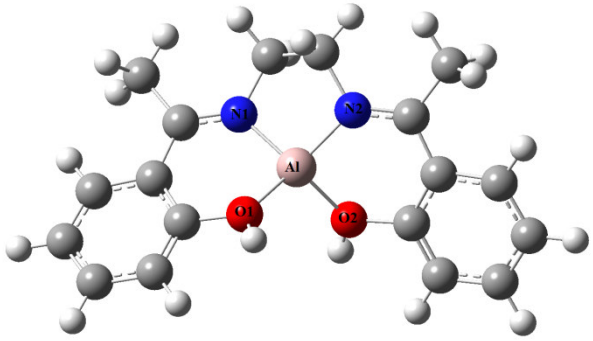

Fig. 8: DFT optimised structure of Al^{3+}**L** complex obtained at B3LYP/6-31G(d,p) level of theory

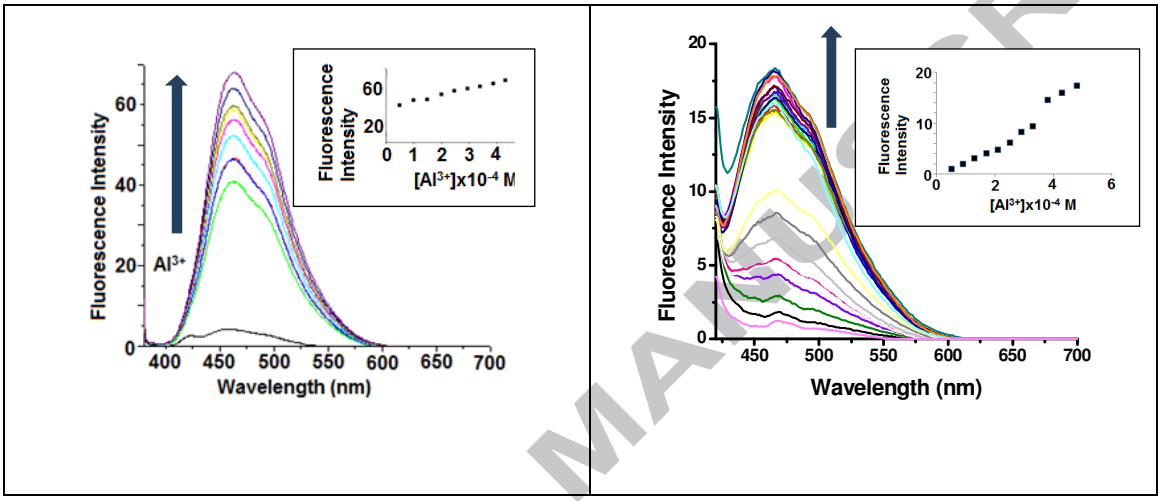

Fig. 9: Fluorescence emission spectra of **L** (50 μM) at different added concentration of Al^{3+}in- [A] BSA-H_2O medium (λ_{em}: 464 nm, λ_{ex}: 370 nm. Inset: Plot of fluorescence intensity versus Al^{3+} concentration in BSA-H_2O medium. [B] BSA-H_2O medium (λ_{em}: 480 nm, λ_{ex}: 410 nm. Inset: Plot of fluorescence intensity versus Al^{3+} concentration in BSA-H_2O medium.

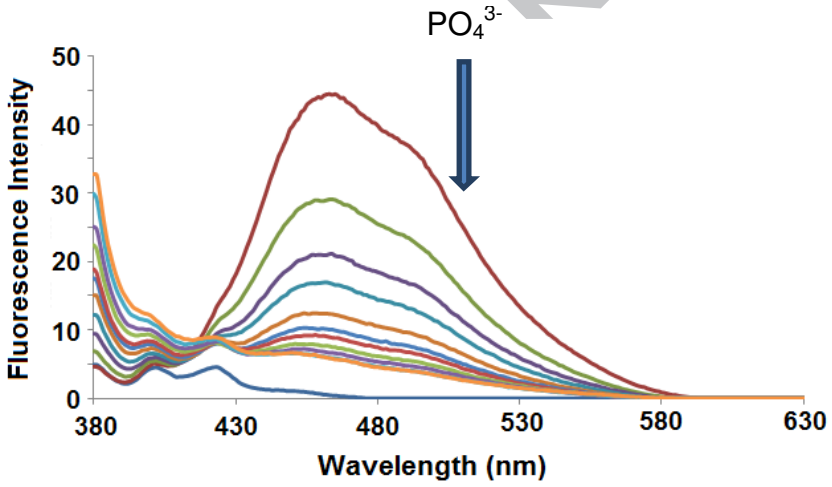

Fig. 10: Effect of PO_4^{3-} ion on the fluorescence spectra of Al^{3+}**L** complex in 1:1 (*v/v*) CH_3OH-H_2O.

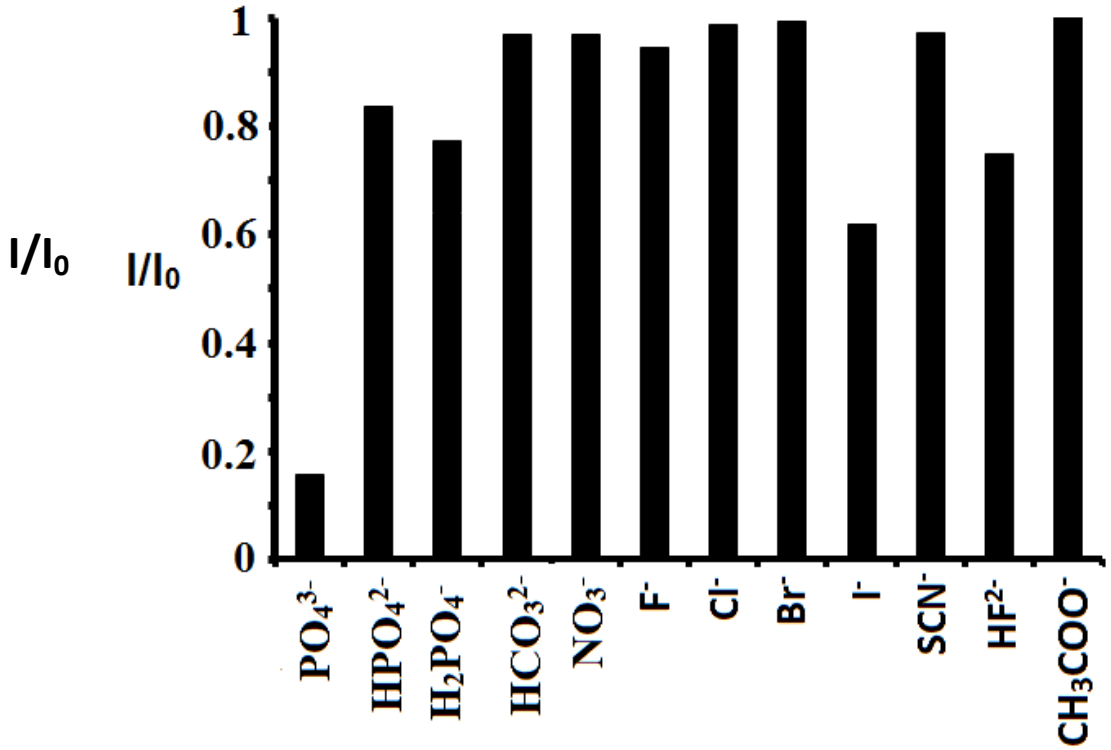

Fig. 11: Effect of different anions on the I/I_o value of Al^{3+}**L** complex in 1:1 (*v/v*) CH_3OH-H_2O. Compared to other anions the fluorescence quenching effect of PO_4^{3-} anion is distinguishably different.

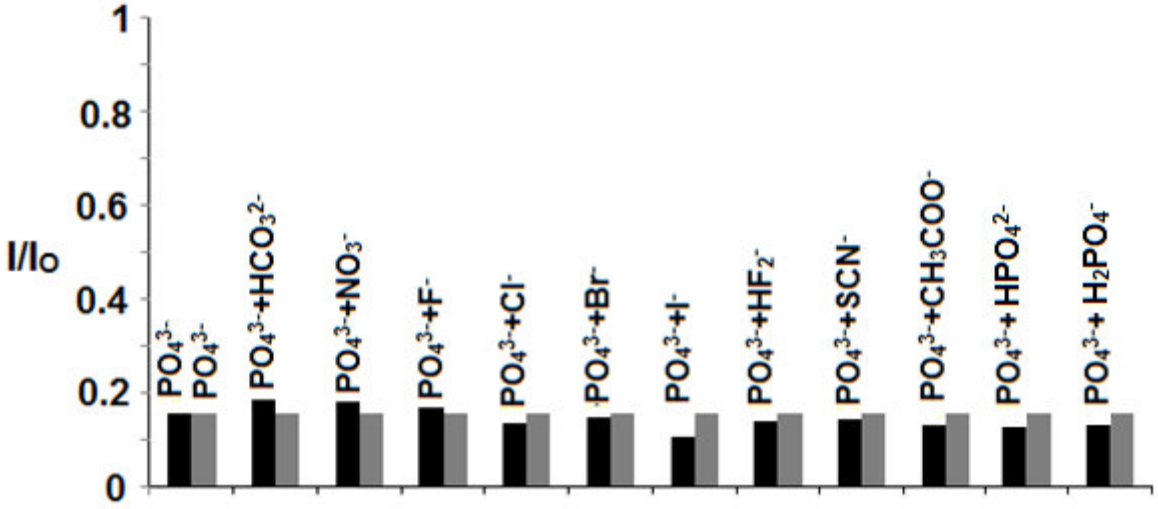

Fig. 12: I/Io values of Al^{3+}**L** complex in presence of PO_4^{3-} alone (grey bars) and in presence of PO_4^{3-} and another anion (black bars). The similar heights of bars indicate that Al^{3+}**L** complex is selective towards PO_4^{3-} in presence of other anions.

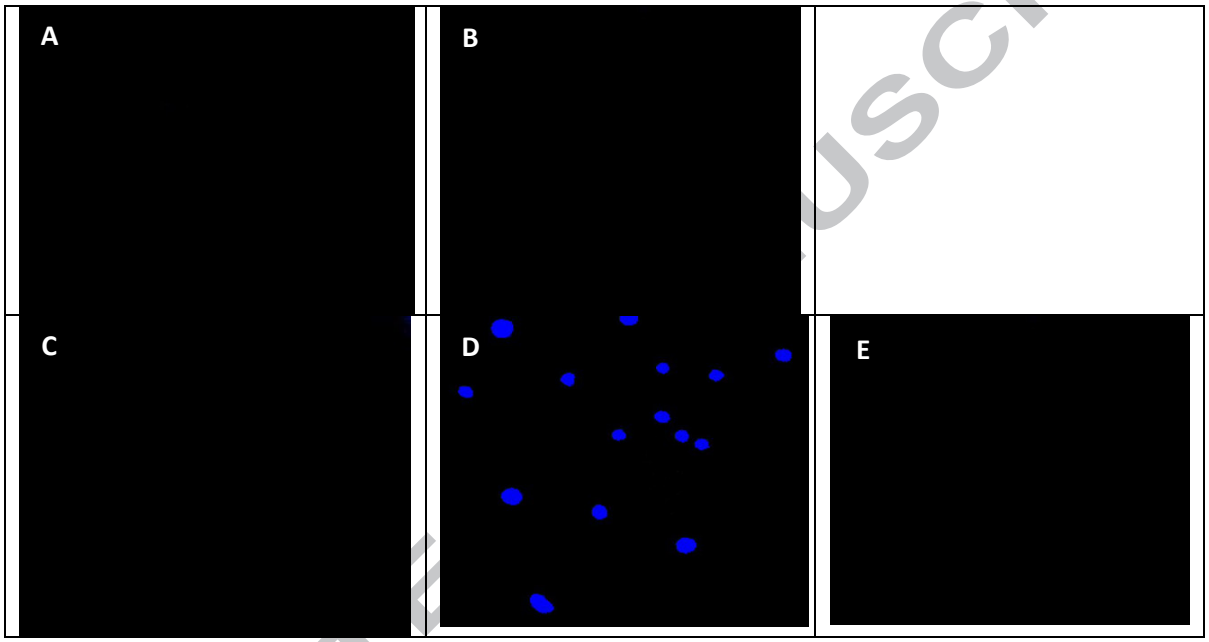

Fig. 13: Fluorescent microscope images of live Rat L6 myoblasts cells (A), cells in presence of **L** (B), cells in presence of Al^{3+} (C), cells in presence of **L** and Al^{3+} (D), cells in presence of **L**, Al^{3+} and Na_2EDTA (E).

Input PO_4^{3-}	Input 2 Al^{3+}	Output
0	0	0
0	1	1
1	0	0
1	1	0

Fig. 14: Truth table for two input (PO_4^{3-} and Al^{3+}) INHIBIT logic gate.

2-Hydroxyacetophenone based Schiff base fluorescent "off-on" sensor for Al^{3+} and its biological cell imaging. Subsequent PO_4^{3-} sensing and INHIBIT logic gate

Jutika Kumar, Ananya Bhowmick, Pradip Kr. Bhattacharyya, Sofia Banu, Diganta Kumar Das

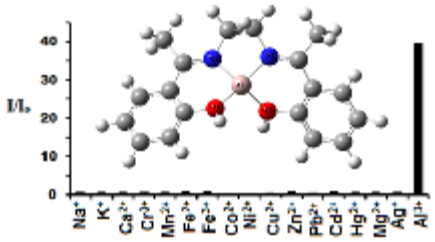

- New fluorescent “off-on” sensor for Al^{3+} in 1:1 (v/v) 1:1 (v/v) CH_3OH:H_2O.
- The sensor:Al^{3+} complex can detect PO_4^{3-} over other anions by fluorescent “on-off” mode.
- The sensor is reversible and applicable for Al^{3+} detection in live cells.
- The sensor shows INHIBIT logic gate behaviour.